



Lipoxygenase-modified Ru-bpy/graphene oxide: Electrochemical biosensor for on-farm monitoring of non-esterified fatty acid



Murugan Veerapandian, Robert Hunter, Suresh Neethirajan *

BioNano Laboratory, School of Engineering, University of Guelph, Guelph ON, Canada N1G 2W1

ARTICLE INFO

Article history:

Received 27 October 2015

Received in revised form

13 November 2015

Accepted 20 November 2015

Available online 21 November 2015

Keywords:

NEFA

On-farm biosensor

Ruthenium (II)-graphene oxide

Soybean lipoxygenase

ABSTRACT

Elevated concentrations of non-esterified fatty acids (NEFA) in biological fluids are recognized as critical biomarkers for early diagnosis of dairy cow metabolic diseases. Herein, a cost-effective, electrochemically active, and bio-friendly sensor element based on ruthenium bipyridyl complex-modified graphene oxide nanosheets ($[\text{Ru}(\text{bpy})_3]^{2+}\text{-GO}$) is proposed as a biosensor platform for NEFA detection. Electrochemical analysis demonstrates that the $[\text{Ru}(\text{bpy})_3]^{2+}\text{-GO}$ electrodes exhibit superior and durable redox properties compared to the pristine carbon and GO electrodes. Target specificity is accomplished through immobilization of the enzyme, lipoxygenase, which catalyzes the production of redox active species from NEFA. Lipoxygenases retain their catalytic ability upon immobilization and exhibit changes to amperometric signals upon interaction with various concentrations of standard NEFA and serum samples. Our study demonstrates that the $[\text{Ru}(\text{bpy})_3]^{2+}\text{-GO}$ electrode has the potential to serve as a biosensor platform for developing a field deployable, rapid, and user-friendly detection tool for on-farm monitoring of dairy cow metabolic diseases.

© 2015 Elsevier B.V. All rights reserved.

1. Introduction

Incidence of Negative Energy Balance (NEB) in dairy cattle caused by increased energy demands at the periparturient period is a serious illness that often affects the livestock production (Jorjong et al., 2014). Circulating Non-Esterified Fatty Acid (NEFA) levels is a good indicator of NEB. During NEB, adipose fat is mobilized as NEFA and transported to the liver to be oxidized or re-esterified into triglycerides. In the liver, excessive supply of NEFA might increase the risk for clinical malignancies such as fatty liver, ketosis, displaced abomasum, metritis, and retained placenta (Ospina et al., 2010a, 2010b). Elevated NEFA in blood plasma also seems detrimental for dairy cow fertility (Garverick et al., 2013). The critical threshold blood NEFA concentrations at pre-partum and post-partum are ≥ 0.3 and ≥ 0.6 mEq/L, respectively (Ospina et al., 2010a). Therefore, constant monitoring of NEFA is an integral part of the clinical aspect of a dairy cow's health management and is of economic value for the live stock producers.

Due to a lack of on-farm diagnostic tests for NEFA, blood samples from dairy cows are collected and sent to off-site laboratories for further testing. NEFA in cows' blood samples are often quantified using high performance liquid chromatography (HPLC), gas chromatography/mass spectrometry (GC/MS), and

liquid chromatography/mass spectrometry (LC/MS) (Miksa et al., 2004). Likewise, matrix-assisted laser desorption ionization/mass spectrometry (MALDI/MS) has received widespread attention in fatty acids analysis. In addition to organic matrixes, inorganic nanostructures of metal and semiconductor particles are also recently studied as matrixes for MALDI/MS, because of their large surface area, thermo-electrical conductivity, and size-dependent light absorption property (Yang and Fujino 2014). Quantification of free fatty acids in human serum was demonstrated using HPLC with fluorescence (Nishikiori et al., 2014), and a chip-based direct-infusion nanoelectrospray ionization source coupled to Fourier transform ion cyclotron resonance MS (Zhang et al., 2014). However, all of the above techniques are expensive, time consuming, require specialized technical operating personnel, and further rely on large laboratory equipment. Two commercial in-vitro enzymatic colorimetric assay kits are available (Roche, 2015; Wako, 2015) for detection of oleic acid and palmitic acid, the major NEFA components in serum. Both methods involve three steps utilizing two enzymes (acyl-CoA synthetase (ACS) and acyl-CoA oxidase (ACOD)) and additional reagent for generating pigment products, which can be quantified by UV-spectrometer at a specific wavelength. Unlike above methods, electrochemical detection approach is not only cost-effective but also suitable for rapid on-farm analysis. Until now, only one report has demonstrated the electrochemical detection of NEFA in human plasma for diabetes management, which is based on two enzymes (ACS and ACOD) modified on multilayer films of poly (dimethyldiallylammonium

* Corresponding author.

E-mail address: sneethir@uoguelph.ca (S. Neethirajan).

chloride) wrapped multi-walled carbon nanotubes assembled on a carbon electrode (Kang et al., 2014). Cows have 11 major blood group systems (A, B, C, F, J, L, M, R, S, T, and Z) unlike four groups in human system owing to different antigen expressions, which makes it complex for accurate determination of NEFA. To authors' knowledge, there is no commercial electrochemical analysis kit available for NEFA, specifically for on-farm testing of clinical samples of dairy animals. Owing to the differences between the blood groups, and the biochemical make up differences between humans and dairy cows, there is a need for diagnostic systems specific to dairy health management. Hence, there is an immediate and dire need to develop a simple, enzymatic, sensitive, and commercially feasible on-farm detection system for rapid determination of NEFA in a cow's biological samples.

Printed carbon electrodes are a well-known, electrochemical-sensing platform for cost-effective disposable devices and have the potential to be used as an in-line sensing system in the robotic milking machine as well as in hand-held diagnostic systems. Among the carbon electrodes, redox active hybrid graphene oxide (GO) materials are a novel electroactive system that recently gained significant attention for various biodetection applications (Jayakumar et al., 2012; Veerapandian and Neethirajan, 2015), due to their cost-efficiency, durable bio-affinity to enzymes, and better electrochemical properties. Similarly, because of its superior photo/electro-chemical nature, catalytic oxidation of $[\text{Ru}(\text{bpy})_3]^{2+}$ is often used in biomarker's detection (Xiao et al., 2014; Veerapandian and Neethirajan, 2015). Herein, a new class of GO material integrated with tris(2,2'-bipyridyl)ruthenium (II) complex ($[\text{Ru}(\text{bpy})_3]^{2+}$) is fabricated and demonstrated as the nanobiosensor platform.

Lipoxygenases are the well-known iron-containing enzymes that catalyze the oxidation of polyunsaturated fatty acids to form a peroxide of the acid. These enzymes are most common in plants and could lead to more efficiency and less cost for scalable biocatalysis. A study supplemented that soybean lipoxygenase-1 (SLO) mediated an oxygenation of monounsaturated fatty acids to enones (Clapp et al., 2001, 2006). Inspired from this study, here SLO is used for the first time to modify $[\text{Ru}(\text{bpy})_3]^{2+}$ -GO for direct electrochemical oxidation of NEFA. Reaction mechanism behind the SLO supported *in situ* electrochemical oxidation of NEFA on the surface of $[\text{Ru}(\text{bpy})_3]^{2+}$ -GO electrode, sensing ability to various concentrations of standard NEFA and serum samples are presented. The entire electrode modifications were performed in a customized screen-printed sensor integrated with working, reference, and counter electrodes on a single chip. Our investigations into $[\text{Ru}(\text{bpy})_3]^{2+}$ -GO-based nanomaterials enabled a durable and amplified electron transfer process at the interface, suitable for biosensing of NEFA. Developed biosensing principle has the potential for on-farm monitoring and detection of metabolic diseases.

2. Experimental

2.1. Materials

Tris(2,2'-bipyridyl)dichlororuthenium(II) hexahydrate, graphite powder (< 20 μm , synthetic), soybean lipoxygenase (type I-B, lyophilized powder, $\geq 50,000$ units/mg) (SLO), L-ascorbic acid (AA), lactic acid solution (LA), uric acid (UA), D(+)-glucose (Glu), and phosphate buffered saline (PBS) were purchased from Sigma-Aldrich. Wako HR series NEFA-HR (2) containing standard NEFA solution (1 mM oleic acid, OA) and enzymatic assay kit were purchased from Wako Diagnostics, CA, USA. Except clinical serum samples, all of the other NEFA analysis were performed using standard OA solution diluted in PBS buffer. Other chemicals were

of analytical grade and used as received without further purification. Milli-Q water (18.2 M Ω) was used in all experiments. Various clinical serum samples of dairy cows, with known concentration of NEFA, were provided as a gift from Animal Health Laboratory, Ontario Veterinary College, University of Guelph.

2.2. Synthesis of GO and functionalization of $[\text{Ru}(\text{bpy})_3]^{2+}$ on GO nanosheets

Aqueous brownish colloidal GO nanosheets were synthesized by harsh oxidation of graphite powder using the modified Hummers method (Hirata et al., 2004). Functionalization of $[\text{Ru}(\text{bpy})_3]^{2+}$ on GO nanosheets was achieved by one-step wet-chemical synthesis, through electrostatic interaction. Typically, 10 mL of aqueous GO nanosheet (1 mg/mL) was magnetically stirred (at 800 rpm) with 10 mL of ethanolic solution of $\text{Ru}(\text{bpy})_3\text{Cl}_2$ (1 mg/mL) at room temperature overnight, protected from light. The as-obtained mixture was centrifuged (at 12,000 rpm for 45 min) and washed repeatedly with anhydrous ethanol and deionized water (DI) to remove the unreacted $[\text{Ru}(\text{bpy})_3]^{2+}$. Isolated $[\text{Ru}(\text{bpy})_3]^{2+}$ -GO nanosheets were dispersed in DI water for further experimentation.

2.3. Construction of SLO-modified GO or $[\text{Ru}(\text{bpy})_3]^{2+}$ -GO electrodes for NEFA detection

A custom-designed carbon screen-printed electrode (SPE) (from Pine research instrumentation, NC, USA) with an area of 2 mm in diameter was used as the substrate for constructing the working electrodes. Integrated U-shaped carbon and the circular Ag/AgCl substrates were used as counter and reference electrodes, respectively. After initial washing with DI water, carbon SPE surface was modified by drop casting 4 μL of aqueous GO or $[\text{Ru}(\text{bpy})_3]^{2+}$ -GO suspension (1 mg/mL) and allowed to evaporate at ambient temperature for 20 min. To ensure uniform coating on the working surface, typically two layers of casting were performed. As-fabricated GO or $[\text{Ru}(\text{bpy})_3]^{2+}$ -GO electrodes were then utilized for electrochemical measurements. For NEFA detection, the above electrodes were further modified by physisorption through drop casting 5 μL of an enzyme SLO (0.25 mg/mL in tris buffer, pH 9). Unbound enzyme on the electrode surface was removed by gentle immersion in the buffer.

2.4. Instrumentation

UV-visible absorbance spectra were measured using Cary 100 UV-vis spectrophotometer (Agilent technologies). μ -Raman spectra were recorded using RENISHAW inVia Raman microscope equipped with a CCD camera and Leica microscope. Measurements were taken using an excitation wavelength of 514 nm, laser power of 10%, exposure time of 30 s, and a short working distance 50 \times objective lens. X-ray photoelectron spectroscopy (XPS) analysis was measured on Omicron XPS spectrometer, a hemispherical analyzer that employs monochromated Al $K\alpha$ radiation ($h\nu = 1486.6$ eV), operating at 12 kV and 300 W. Transmission electron microscope (TEM) images were obtained from FEI-Tecani G2, operating at 200 kV. Scanning electron microscope (SEM) images were obtained using FEI Inspect S50 at an accelerating voltage of 15 kV. Elemental mapping was done using Oxford X-Max20 silicon drift detector and Aztec software. All electrochemical measurements were performed using SP-150 potentiostats, Bio-Logic instruments.

3. Results and discussion

3.1. Characterization of GO and $[\text{Ru}(\text{bpy})_3]^{2+}$ -GO nanostructures

As shown in Fig. 1(A), UV-vis spectrum of GO exhibit the π - π^* band of the polyaromatic C-C at 230 nm (Veerapandian et al., 2014). Characteristic intra-ligand transition $\pi \rightarrow \pi^*$, bpy $\pi \rightarrow \pi_1^*$ transition, and metal-to-ligand charge-transfer (MLCT) bands of $[\text{Ru}(\text{bpy})_3]^{2+}$ are observed at 243, 285, and 450 nm, respectively (Mori et al., 2010). A shoulder peak at 420 nm is also associated with MLCT ($t_{2g}(\text{Ru}) \rightarrow \pi^*(\text{bpy})$ transitions). Due to the better optical absorption of $[\text{Ru}(\text{bpy})_3]^{2+}$, the hybrid $[\text{Ru}(\text{bpy})_3]^{2+}$ -GO dispersion also exhibits the above-mentioned peaks. Observed notable broadness in the individual bands of $[\text{Ru}(\text{bpy})_3]^{2+}$ supports the possible interaction with active groups of GO and its influence in the inherent absorbance.

Carbon lattice phase of GO studied from Raman spectroscopy (Fig. 1B) shows the characteristic D- and G-bands, at 1353 cm^{-1} and 1596 cm^{-1} corresponding to A_{1g} symmetry and E_{2g} phonon mode, respectively (Krishnamoorthy et al., 2013). In addition to intrinsic D- and G-bands, $[\text{Ru}(\text{bpy})_3]^{2+}$ -GO nanosheets exhibit a band at 1481 cm^{-1} attributed to C-N stretching vibrations of

bipyridyl groups (Xiao et al., 2013). The intensity ratio of $I_{(D)}/I_{(G)}$ for GO and $[\text{Ru}(\text{bpy})_3]^{2+}$ is 0.82 and 0.74, respectively, implying that $[\text{Ru}(\text{bpy})_3]^{2+}$ influenced the graphitic sp^2 carbon domains on GO. The average crystallite size of sp^2 domains in GO and $[\text{Ru}(\text{bpy})_3]^{2+}$ -GO, calculated according to Tuinstra and Koenig's equation (Tuinstra and Koenig 1970), is 20.42 and 22.63, respectively.

The deconvoluted C1s peaks of pristine GO are presented in Fig. 1C (i). Peaks centered at the binding energies of 288.5, 287, 286.2, and 285 eV are attributed to the oxygenated functional groups such as carboxyl, carbonyl, epoxy, and hydroxide, respectively (Koinuma et al., 2012, Krishnamoorthy et al., 2013). Peak centered at 284.2 eV is assigned to the non-oxygenated carbon lattice groups such as C=C, C-C, and C-H (Krishnamoorthy et al., 2013). As shown in Fig. 1C (ii), functionalization of $[\text{Ru}(\text{bpy})_3]^{2+}$ significantly altered the chemical groups of GO, that include the presence of a new peak centered at 281.1 eV, ascribed to $\text{Ru}3d_{5/2}$ (Agnes et al., 2009). In addition to a minor shift in the binding energies of epoxy (from 286.2 to 285.7 eV) and hydroxyl (from 285 to 285.2 eV) groups, absence of carboxyl and carbonyl group signals indicate that the $[\text{Ru}(\text{bpy})_3]^{2+}$ chemically interact on the surface of GO. This result is further supported by the elemental

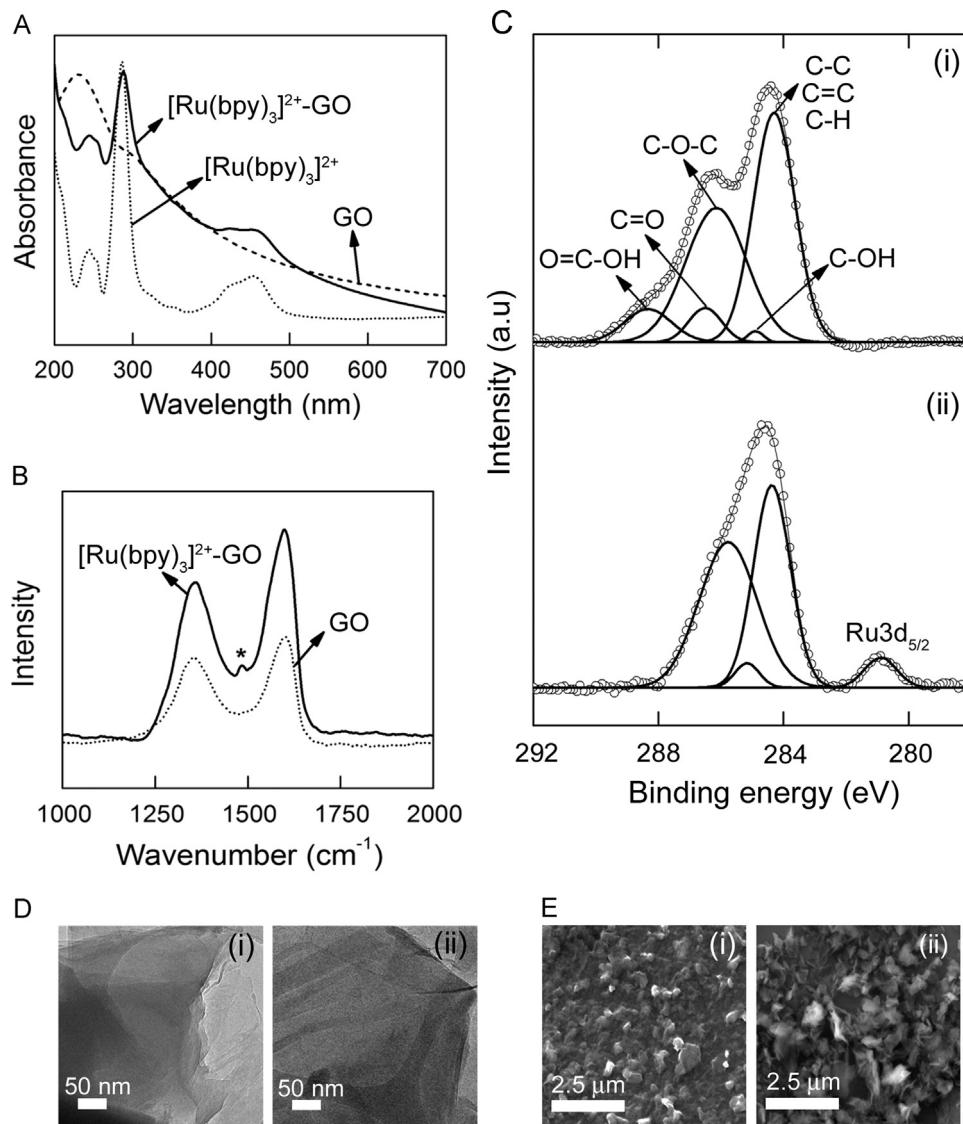


Fig. 1. (A) UV-vis absorbance spectra, (B) Raman spectra (asterisk denotes the C-N of bipyridyl groups), (C) XPS spectra of C1s, (D) TEM, and (E) SEM images of (i) pristine GO and (ii) $[\text{Ru}(\text{bpy})_3]^{2+}$ -GO.

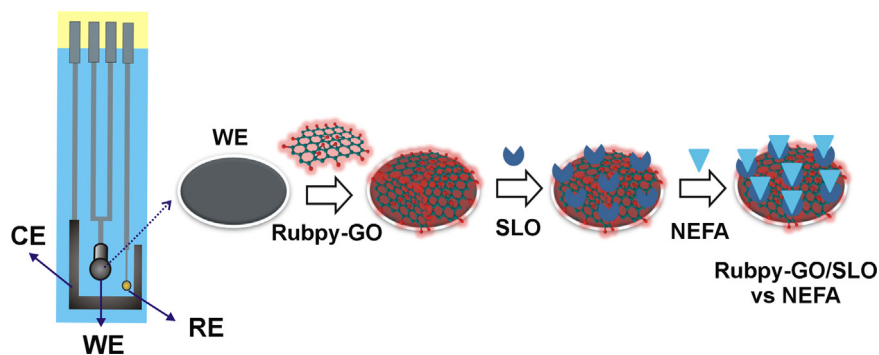


Fig. 2. Illustration of customized SPE describing the SLO modification on Rubpy-GO electrode and its reaction with NEFA sample. Rubpy denotes $[\text{Ru}(\text{bpy})_3]^{2+}$. WE: working electrode, CE: counter electrode and RE: reference electrode.

mapping analysis, provided in the supporting information (Fig. S1 and S2). Few layers of ultra-thin sheets of GO and $[\text{Ru}(\text{bpy})_3]^{2+}$ -GO observed from TEM, and microclusters of sheetlike structures with larger network studied from SEM are presented in Fig. 1 (D) and (E), respectively.

3.2. Construction of $[\text{Ru}(\text{bpy})_3]^{2+}$ -GO based sensor platform

Due to its multiple oxygenated functional groups, GO is generally believed to be an insulating material. Considering the cost-effective and effortless scalable synthesis, significant efforts were made to improve the electrochemical properties of GO so they are suitable for biosensor. Among these, elemental doping and functionalization of hybrid inorganic/organic structures, chemical reduction, and photoirradiation are recent approaches. Such modified GO-based materials have been demonstrated for a range of biosensors that include, homocysteine (Kannan et al., 2013), quercetin (Veerapandian et al., 2014), estriol (Cincotto et al., 2015), botulinum neurotoxin A (Chan et al., 2015), and *Listeria monocytogenes* (Veerapandian and Neethirajan 2015) to name a few. Herein, as shown in Fig. 2, at first the working surface (2 mm in diameter) of customized SPE was modified with $[\text{Ru}(\text{bpy})_3]^{2+}$ -GO through drop casting method. Afterward, enzyme SLO was immobilized for direct electrochemical detection of NEFA. Due to its matrix-like structure with abundant chemical groups, GO-based hybrid materials readily adhere onto the electrode surface. Notably, using screen-printing technology, the suspension of prepared nanomaterials could be conveniently scalable for mass production with high precision. Advantages of SPE include miniaturization, ease of operation, portability, reliability, and modest fabrication cost.

3.3. Electrochemical properties of $[\text{Ru}(\text{bpy})_3]^{2+}$ -GO electrodes for NEFA detection

The cyclic voltammogram (CV) of bare carbon-, GO-, and $[\text{Ru}(\text{bpy})_3]^{2+}$ -GO nanosheets-modified electrodes measured under PBS buffer (7.4) at a scan rate of 20 mV/s, without NEFA were provided in supporting information (Fig. S3). It has been observed that bare carbon- and GO-modified electrodes don't exhibit characteristic redox behavior. Interestingly, the $[\text{Ru}(\text{bpy})_3]^{2+}$ -GO nanosheets' modified carbon SPE showed a well-defined peak centered at $E_{pa} = +0.055$ V and $E_{pc} = -0.1$ V vs Ag/AgCl, which is attributed to the redox behavior of $\text{Ru}^{\text{II}}/\text{Ru}^{\text{III}}$. The observed oxidation potential (+0.055 V) is comparably less positive than the previously reported, carbon paste, ITO, and graphene-modified glassy carbon, electrodes (Wohnrath et al., 2005, 2006; Xu et al., 2015). Such enhanced redox response is mainly due to the stable interaction of $[\text{Ru}(\text{bpy})_3]^{2+}$ with the basal plane and the edges of GO sheets. Therefore, a significant alteration in the carbon/oxygen

atomic ratio creates new sp^3 and sp^2 domains on the lattice network and its derived electroactive charge carriers. The scan rate dependence of the CV response from $[\text{Ru}(\text{bpy})_3]^{2+}$ -GO electrode was examined (Fig. S4) and it was found that the redox current is proportional to the scan rate ($v^{1/2}$). Representative anodic peak current fit exhibit a correlation co-efficient of 0.997, suggesting the surface-confined reaction process.

CV study of pristine SLO modified $[\text{Ru}(\text{bpy})_3]^{2+}$ -GO electrode in PBS buffer exhibits a broad anodic peak centered at +0.11 V. Absence of inherent cathodic peak (under this potential window) attributed to the cycle Ru^{III} to Ru^{II} is perhaps due to the existence of SLO, which hinders the reduction reaction at the electrode interface. Upon interaction with NEFA, the anodic peak current generated from the $[\text{Ru}(\text{bpy})_3]^{2+}$ -GO/SLO electrode is noticeably higher than the pristine one, with a minor shift in the peak potential (from +0.11 to +0.125 V). This implies that an electrochemical oxidation of NEFA is feasible at the SLO supported $[\text{Ru}(\text{bpy})_3]^{2+}$ -GO electrode. The relevant CVs of SLO-modified bare carbon and GO electrodes in absence and presence of standard NEFA samples were compared in Fig. 3A. Preliminary voltammetric investigations showed that the change of anodic peak current, specifically at +0.17 V, is an optimal potential to monitor the sensing ability. Hence, an applied potential of +0.17 V was used for amperometric sensing of NEFA samples. Presence of SLO on the surface of $[\text{Ru}(\text{bpy})_3]^{2+}$ -GO readily oxidizes the free NEFA and hence supplies electrons to the electrode. Plausible electrochemical catalytic reaction of SLO and inherent redox reaction of an electrode are explained in Fig. S5. Chronoamperometric response of the $[\text{Ru}(\text{bpy})_3]^{2+}$ -GO/SLO electrodes to different concentrations of OA (NEFA) and its relevant calibration plot are illustrated in Fig. 3(B) and (C), which shows a high sensitivity of $40.5 \mu\text{A mM}^{-1}$, in the linear detection range of 0.1–1.0 mM. Further, specificity of the proposed electrode was evaluated in presence of various potential interferents, viz., AA, LA, UA, and Glu. To ensure the specificity, a three-fold increase of interferent's concentration (1.2 mM) was utilized. As observed in Fig. 3D, the amperometric response against the 0.4 mM concentration of OA is still better than the studied interferent's concentration, indicating that the enzyme SLO on the surface of $[\text{Ru}(\text{bpy})_3]^{2+}$ -GO selectively oxidizes the standard NEFA, resulting in an uninterrupted electron transfer process. Further, the practical application of the proposed electrode toward real clinical samples for monitoring NEFA was explored. At first, different dairy cows suspected with NEB were selected and their respective serum samples of various NEFA concentrations were obtained from Animal Health Laboratory of the University of Guelph. The amperometric sensing ability of the $[\text{Ru}(\text{bpy})_3]^{2+}$ -GO/SLO electrode for NEFA was measured with the selected serum samples (within critical threshold), such as 0.38, 0.5, 0.75, and 1.0 mM, respectively. Compared to standard NEFA samples (Fig. 3C), the current sensitivity of the electrodes with

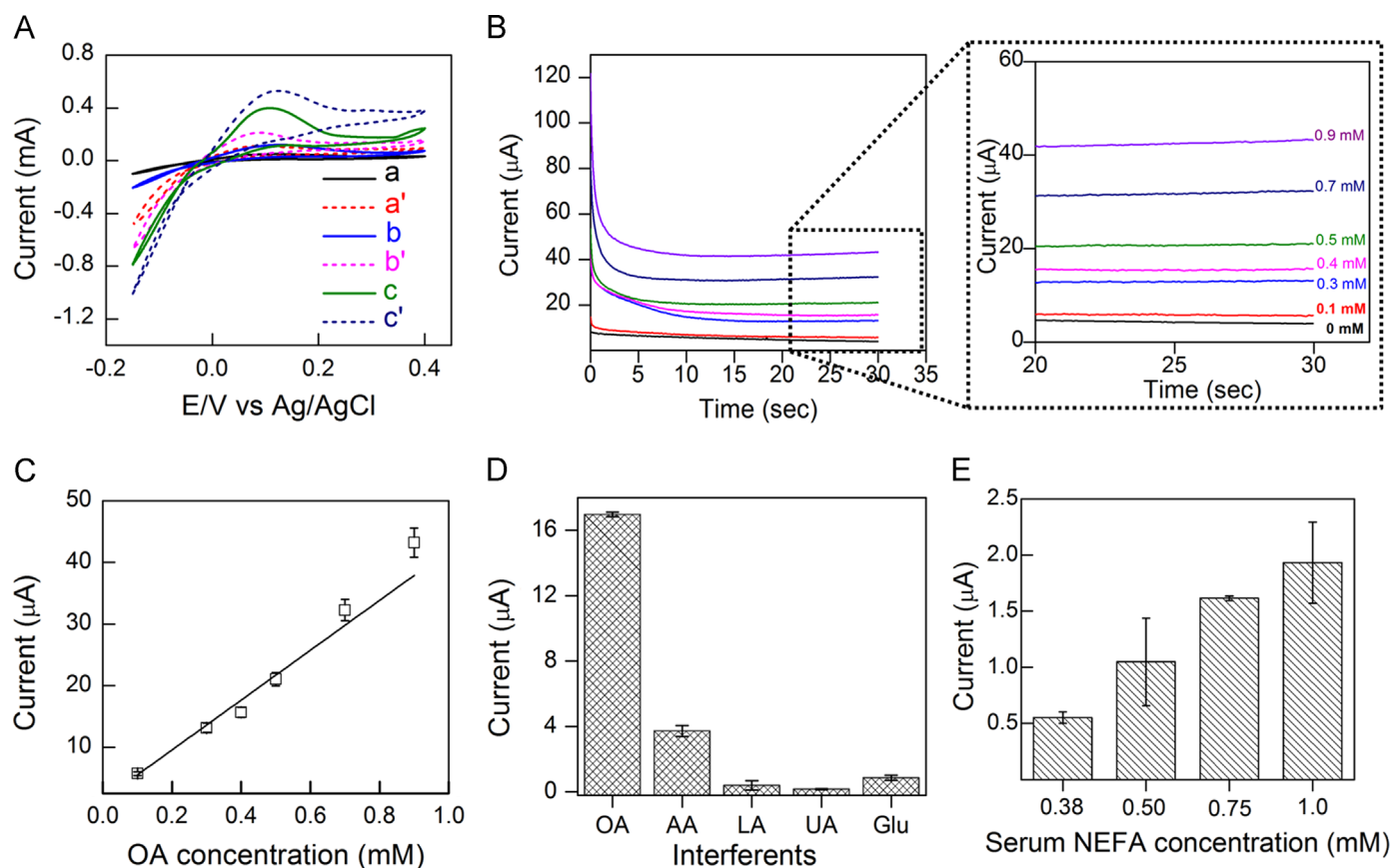


Fig. 3. (A) CVs of SLO modified electrodes, (a) bare carbon SPE, (b) GO/SPE and (c) $[\text{Ru}(\text{bpy})_3]^{2+}$ -GO/SPE measured in PBS buffer (pH 7.4) at a scan rate of 20 mV/s, in absence of OA; (a'), (b') and (c') represents the CV of bare carbon SPE, GO-SPE and $[\text{Ru}(\text{bpy})_3]^{2+}$ -GO-SPE, respectively, measured in presence of OA (0.4 mM). (B) Chronoamperometric curves of $[\text{Ru}(\text{bpy})_3]^{2+}$ -GO/SLO electrodes measured with various concentrations of OA samples. (C) Representative calibration curve fit illustrates the amperometric current of $[\text{Ru}(\text{bpy})_3]^{2+}$ -GO/SLO against various concentrations of OA in PBS (pH 7.4). (D) Amperometric histogram of $[\text{Ru}(\text{bpy})_3]^{2+}$ -GO/SLO electrode measured in the presence of OA (0.4 mM) and interferents (1.2 mM). (E) Amperometric response from four different serum samples measured at $[\text{Ru}(\text{bpy})_3]^{2+}$ -GO/SLO electrodes. All the amperometric measurements were recorded at an applied bias of +0.17 V. Each data point presented in (C), (D) and (E) indicates the mean of three successive measurements at different electrodes ($n=3$).

serum samples decreased, perhaps due to the presence of multiple serum components. However, as shown in Fig. 3E, the changes in individual current values and serum NEFA concentrations have a relationship suitable for potential detection application. Moreover, the obtained results are certainly consistent with WAKO kit values compared in Fig. S6. The electrochemical approach described herein has been shown to be fast (<1 min) and efficient in comparison with conventional assays available in the literature, as discussed in the introduction. Further, using screen-printed electrode system, the sensing mechanism can be effectively integrated and is feasible for early diagnosis of metabolic diseases and to provide point-of-care for on-site monitoring. Proposed design would require no further sample pretreatment. Optimal calibration of transduction signal will improve the real-time detection of selective markers.

4. Conclusions

A field deployable biosensor platform based on $[\text{Ru}(\text{bpy})_3]^{2+}$ -GO nanosheet for direct electrochemical detection of NEFA is demonstrated. Immobilization of lipoxigenase on the electrode surface selectively catalyzes the NEFA into fatty enones and influences the inherent redox reaction at the interface. Lipoxigenase-modified electrode system possesses high specificity and shows excellent linear dependence toward various concentrations of the standard NEFA as well as serum samples. Proposed

enzymatic amperometric biosensor is relatively simple and rapid in analysis, without the need for sample pretreatments. Demonstrated sensing approach in a single screen-printed chip finds potential application especially in on-farm point-of-care diagnostics.

Acknowledgments

The authors sincerely thank the Natural Sciences and Engineering Research Council of Canada (Grant# 400929), Ontario Ministry of Research and Innovation (Grant# 051455), and the Dairy Farmers of Canada (Grant# 051520) for funding this study.

Appendix A. Supplementary material

Supplementary data associated with this article can be found in the online version at <http://dx.doi.org/10.1016/j.bios.2015.11.058>.

References

- Agnes, C., Arnault, J.C., Omnes, F., Jousselme, B., Billon, M., Bidan, G., Mailley, P., 2009. *Phys. Chem. Chem. Phys.* 11, 11647–11654.
- Chan, C.Y., Guo, J., Sun, C., Tsang, M.K., Tian, F., Hao, J., Chen, S., Yang, M., 2015. *Sens. Actuators B* 220, 131–137.
- Cincotto, F.H., Canevari, T.C., Machado, S.A.S., Sánchez, A., Barrio, M.A.R., 2015.

- Electrochim. Acta 174, 332–339.
- Clapp, C.H., Senchak, S.E., Stover, T.J., Potter, T.C., Findeis, P.M., Novak, M.J., 2001. *J. Am. Chem. Soc.* 123, 747–748.
- Clapp, C.H., Strulson, M., Rodriguez, P.C., Lo, R., Novak, M.J., 2006. *Biochemistry* 45, 15884–15892.
- Jayakumar, K., Rajesh, R., Dharuman, V., Venkatasan, R., Hahn, J.H., Karutha Pandian, S., 2012. *Biosens. Bioelectron.* 31, 406–412.
- Garverick, H.A., Harris, M.N., Vogel-Bluel, R., Sampson, J.D., Bader, J., Lamberson, W. R., Spain, J.N., Lucy, M.C., Youngquist, R.S., 2013. *J. Dairy Sci.* 96, 181–188.
- Hirata, M., Gotou, T., Horiuchi, S., Fujiwara, M., Ohba, M., 2004. *Carbon* 42, 2929–2937.
- Jorjong, S., van Kneysel, A.T.M., Verwaeren, J., Val Lahoz, M., Bruckmaier, R.M., De Baets, B., Kemp, B., Fievez, V., 2014. *J. Dairy Sci.* 97, 7054–7064.
- Kannan, P., Maiyalagan, T., Sahoo, N.G., Opallo, M., 2013. *J. Mater. Chem. B* 1, 4655–4666.
- Kang, J., Hussain, A.T., Catt, M., Trenell, M., Hagggett, B., Yu, E.H., 2014. *Sens. Actuators B – Chem.* 190, 535–541.
- Koinuma, M., Ogata, C., Kamei, Y., Hatakeyama, K., Tateishi, H., Watanabe, Y., Taniguchi, T., Gezuhara, K., Hayami, S., Funatsu, A., Sakata, M., Kuwahara, Y., Kurihara, S., Matsumoto, Y., 2012. *J. Phys. Chem. C* 116, 19822–19827.
- Krishnamoorthy, K., Veerapandian, M., Yun, K.S., Kim, S.J., 2013. *Carbon* 53, 38–49.
- Miksa, I.R., Buckley, C.L., Poppenga, R.H., 2004. *J. Vet. Diagn. Invest.* 16, 139–144.
- Mori, K., Kawashima, M., Cheand, M., Yamashita, H., 2010. *Angew. Chem. Int. Ed.* 49, 8598–8601.
- Nishikiori, M., Iizuka, H., Ichiba, H., Sadamoto, K., Fukushima, T., 2014. *J. Chromatogr. Sci.* 53, 537–541.
- Ospina, P.A., Nydam, D.V., Stokol, T., Overton, T.R., 2010a. *J. Dairy Sci.* 93, 546–554.
- Ospina, P.A., Nydam, D.V., Stokol, T., Overton, T.R., 2010b. *J. Dairy Sci.* 93, 1596–1603.
- Roche, (<https://e-labdoc.roche.com/LFR>) PublicDocs/ras/11383175001 en 09.pdf retrieved on 13/05/2015.
- Tuinstra, F., Koenig, J.L., 1970. *J. Chem. Phys.* 53, 1126–1130.
- Veerapandian, M., Seo, Y.T., Yun, K.S., Lee, M.-H., 2014. *Biosens. Bioelectron.* 58, 200–204.
- Veerapandian, M., Neethirajan, S., 2015. *RSC Adv.* 5, 75015–75024.
- Wako, (http://www.wakodiagnosics.com/r_nefa.html) pdf retrieved on 13/05/2015.
- Wohnrath, K., Pessoa, C.A., dos Santos, P.M., Garcia, J.R., Batista, A.A., Oliveira Jr, O.N., 2005. *Prog. Solid State Chem.* 33, 243–252.
- Wohnrath, K., dos Santos, P.M., Sandrino, B., Garcia, J.R., Batista, A.A., Oliveira Jr, O. N., 2006. *J. Braz. Chem. Soc.* 17, 1634–1641.
- Xiao, F.N., Wang, M., Wang, F.B., Xia, X.H., 2014. *Small* 10, 706–716.
- Xiao, B., Wang, X., Huang, H., Zhu, M., Yang, P., Wang, Y., Du, Y., 2013. *J. Phys. Chem. C* 117, 21303–21311.
- Xu, Y., Cao, M., Liu, H., Zong, X., Kong, N., Zhang, J., Liu, J., 2015. *Talanta* 139, 6–12.
- Yang, M., Fujino, T., 2014. *Anal. Chem.* 86, 9563–9569.
- Zhang, Y., Qiu, L., Wang, Y., Qin, X., Li, Z., 2014. *Analyst* 139, 1697–1706.